
This is an electronic reprint of the original article.
This reprint may differ from the original in pagination and typographic detail.

Sun, Haibin; Liu, Xiaolong; Zhao, Li; Jia, Jianxin; Jiang, Changhui; Xiao, Jiamin; Chen, Yuwei; Xu, Long; Duan, Zhiyong; Rao, Peng; Sun, Shengli

Mid-long wavelength infrared absorptance of hyperdoped silicon via femtosecond laser microstructuring

Published in:
Optics Express

DOI:
[10.1364/OE.446283](https://doi.org/10.1364/OE.446283)

Published: 17/01/2022

Document Version
Publisher's PDF, also known as Version of record

Published under the following license:
CC BY

Please cite the original version:
Sun, H., Liu, X., Zhao, L., Jia, J., Jiang, C., Xiao, J., Chen, Y., Xu, L., Duan, Z., Rao, P., & Sun, S. (2022). Mid-long wavelength infrared absorptance of hyperdoped silicon via femtosecond laser microstructuring. *Optics Express*, 30(2), 1808-1817. <https://doi.org/10.1364/OE.446283>

This material is protected by copyright and other intellectual property rights, and duplication or sale of all or part of any of the repository collections is not permitted, except that material may be duplicated by you for your research use or educational purposes in electronic or print form. You must obtain permission for any other use. Electronic or print copies may not be offered, whether for sale or otherwise to anyone who is not an authorised user.



Mid-long wavelength infrared absorptance of hyperdoped silicon via femtosecond laser microstructuring

HAIBIN SUN,^{1,2,3} XIAOLONG LIU,⁴  LI ZHAO,³ JIANXIN JIA,²
CHANGHUI JIANG,² JIAMIN XIAO,³ YUWEI CHEN,^{2,*}  LONG XU,⁵
ZHIYONG DUAN,⁶ PENG RAO,¹ AND SHENGLI SUN¹

¹Key laboratory of Intelligent Infrared Perception Chinese Academy Science (CAS), Shanghai Institute of Technical Physics, Chinese Academy Science (CAS), Shanghai 200043, China

²Department of Remote Sensing and Photogrammetry, Finnish Geospatial Research Institute, Kirkkonummi FI-02431, Finland

³State Key Laboratory of Surface Physics and Department of Physics, Fudan University, Shanghai 200433, China

⁴Department of Electronics and Nanoengineering, Aalto University, Tietotie 3, Espoo FI-02150, Finland

⁵School of Physical Science and Technology, Southwest University, Chongqing 400715, China

⁶School of Physical Engineering, Zhengzhou University, Zhengzhou 450001, China

*yuwei.chen@nls.fi

Abstract: Hyperdoped silicon (hSi) fabricated via femtosecond laser irradiation has emerged as a promising photoelectric material with strong broadband infrared (IR) absorption. In this work, we measured the optical absorptance of the hSi in the wavelength of 0.3–16.7 μm . Unlike the near to mid wavelength IR absorption, the mid-long wavelength IR (M–LWIR) absorption is heavily dependent on the surface morphology and the dopants. Furthermore, calculations based on coherent potential approximation (CPA) reveal the origin of free carrier absorption, which plays an important role in the M–LWIR absorption. As a result, a more comprehensive picture of the IR absorption mechanism is drawn for the optoelectronic applications of the hSi.

© 2022 Optica Publishing Group under the terms of the [Optica Open Access Publishing Agreement](#)

1. Introduction

In the past half-century, microelectronic technology has greatly promoted the development of information technology, especially for microelectronic devices based on silicon (Si) and III-V group semiconductors. The silicon material is more compatible with the current mature complementary-metal-oxide-semiconductor (CMOS) technology at a low cost. However, the bandgap of Si (1.12 eV) limits its application, especially for the infrared (IR) optoelectronic integration devices. To meet this challenge, various methods have been developed to modify the intrinsic band structure of Si via the intentional introduction of defects [1–4]. Femtosecond (fs) laser irradiation, as an effective surface modification technique to functionalize Si materials, has successfully introduced supersaturated impurities or dopants (*e.g.*, S, Se, Te, N, Au, and Ag) in the surface layer at concentrations of 10^{19} – 10^{20} atoms/cm³ (3–4 orders of magnitude above the equilibrium solid solubility limit) [2,5–7]. Simultaneously, a forest of quasi-ordered micrometer-sized conical spikes could also be created on the surface [8]. Thus, this fs-laser irradiated Si has also been named black silicon or hyperdoped silicon (hSi) [2,5,9]. The supersaturated impurities doped in silicon could form intermediate bands (IBs) in the bandgap of Si and induce strong below-bandgap optical absorptance and photocurrent generation [10–12]. Moreover, the surface microstructures further enhance the light absorptance through multireflection. Overall, these characteristics highlight the potential applications of the hSi such as high-efficiency solar

cells [13,14], infrared photodiodes [15,16], novel photo-assisted gas sensors [17–20], and plane blackbody with ultrahigh emissivity [21].

Although the hSi exhibits strong sub-bandgap absorption at wavelengths up to longer than 15 μm and photoconductivity spectra in wavelength of 2–21 μm , photodiodes based on hSi exhibit responsivity only up to around 1.5 μm [9,15,22]. The large difference in the photo-electric properties between the wavelength of shorter and longer than 1.5 μm implies that there should be different mechanisms for the optical absorption in different wavelengths. It has been identified that bandgap or intrinsic absorption, impurity level-to-band absorption, and free carrier absorption are the main mechanisms for the optical absorbance of the hSi [23]. More than 99% absorbance in the visible to near-infrared (vis–NIR, 0.3–1.1 μm) could be obtained from the synergy of surface microstructures and intrinsic absorption, and as high as 90% absorbance in near to short wavelength IR (NIR–SWIR, 1.1–2.5 μm) has been demonstrated due to the presence of the impurity level-to-band absorption [8,24]. Furthermore, the mid to long wavelength infrared (M–LWIR, 3–16 μm) absorbance has been randomly reported to be influenced by surface morphology, doping impurities, nano-particles, coating film in the surface layer and many other factors [24–27]. However, considering the broad wavelength range in IR, the complete picture of the optical absorption mechanism for IR is not so clear. It has been confirmed there is an upper bound in mid-wavelength infrared (MWIR) for the impurity level-to-band absorption [24–27], so the strong absorption in longer wavelengths could not be explained by the IBs induced by supersaturated dopants. Therefore, a further clarification of M–LWIR absorption mechanism is a crucial step for the optoelectric applications in IR range based on the hSi.

In this work, we fabricate hSi samples via fs-laser irradiation in sulfur hexafluoride (SF_6), nitrogen trifluoride (NF_3), and nitrogen (N_2) gas ambient, denoted SF_6 -, NF_3 - and N_2 -hSi, introducing super-saturated S atoms, N atoms, and N_2 molecules, respectively [8,10,28]. We measure the optical absorbance in the wavelength range of 0.3–16.7 μm , and demonstrate large difference of M–LWIR absorbance from shorter wavelengths before and after annealing. Furthermore, the effects of surface morphology and the dopants are studied by fabricating hSi samples with different laser fluences and by performing chemical etching experiment. In addition, the CPA calculations implemented in the nano-electronic device simulator (NANODSIM) package based on disordered doping structure reveals the origin of free carrier absorption, which should be one of the most important factors for the M–LWIR absorption.

2. Experiment and calculation

The Czochralski (CZ) silicon wafer with 250 μm thickness (P-type, (100), 1–3 Ω/cm^2) was placed on a mobile panel in a stainless-steel vacuum chamber. The chamber was filled with 70 kPa gas atmosphere of SF_6 , NF_3 , or N_2 . The silicon wafer was irradiated by a Yb:KGW fs-laser that delivered a 1 kHz train of 190 fs laser pulse at a wavelength of 515 nm. The pulsed laser beam was focused to a spot size of 60 μm in diameter on the silicon surface with a 250 mm focal length lens. An area of approximately 10 \times 10 mm^2 textured surfaces was raster-scanned at a speed of 500 $\mu\text{m}/\text{s}$, and any given spot on the wafer is exposed to an average of 350 shots. Different laser fluences on the Si surface were obtained by adjusting the output power of the laser and the speed of the raster scanning, so that the height of the conic spikes on the surface layer could be modulated. With the fs-laser irradiation at the fluence of 12.1 kJ/m^2 , 12.3 kJ/m^2 and 15 kJ/m^2 in the atmosphere of SF_6 , NF_3 , N_2 , we obtained SF_6 -, NF_3 - and N_2 -hSi covered with quasi-period conical spikes of similar average height (h). More details on the fs-laser doping procedure and experimental setup was described in Ref. [5].

After laser texturing, rapid thermal annealing (RTA) was performed for certain samples in forming N_2 gas at 800 K for 5 min. The total hemispherical (specular and diffuse) reflectance (R) and transmittance (T) spectra of these hyperdoped samples were measured to obtain its absorbance ($A = 1 - R - T$). A UV-vis-NIR spectrophotometer (Varian Cary 5 E) was used to

collect the visible (vis) and NIR (0.25–2.5 μm) absorptance data, and a Fourier Transformed-Infrared (FTIR) spectrometer (Brucker Equinox 55) was used for measurements of IR spectra in 2.5–16.7 μm . Both spectrophotometer and FTIR spectrometer are equipped with an integrating sphere. Scanning electron microscopy (SEM) was used to observe the surface morphology and measurement the characteristic dimensions of microstructures on the surface layer. To measure the characteristic dimensions, the SEM was observed at an angle of 45° to the surface. Thus, the high (h) of the quasi-periodic spikes on the surface were obtained by the observed heights divided by $\cos 45^\circ$. The chemical etching of hSi surface was done by using 10% KOH solution at 60°C for a controlled time duration, with an etching speed of about 480 nm/min for the Si (100) surface [29]. The presence sulfur dopants in the etched samples was determined by the X-ray photoelectron spectroscopy (XPS).

The hyperdoped impurities in silicon were theoretically investigated by CPA method, and the band structures of the hSi were calculated. The CPA method is based on the non-equilibrium Green function and implemented in the density functional theory (DFT) within the tight binding linear muffin-tin orbital (TB-LMTO) under atomic sphere approximation (ASA), more details can be found elsewhere [30,31]. A modified Becke–Johnson (MBJ) semi-local exchange potential was proposed to provide an accurate band gap, and the above LMTO-CPA-MBJ self-consistent DFT calculation is implemented in the NANODSIM package. Compared with the supercell method based on the Vienna Ab-initio Simulation Package (VASP), the CPA method is more suitable for the low doping concentration and the disorder effect, which are the most obvious characteristics of dopants in the hSi [11]. For the system of crystalline Si, the K-point samplings are $3\times 3\times 3$ and $2\times 2\times 2$ in the irreducible Brillouin zone (BZ), which included 64 and 216 atoms and the corresponding sulfur doping concentration was 1.56% and 0.46%, respectively. Changing the chance of atomic site to modulate the disorder of the model, e.g., for the $S_x\text{Si}_{1-x}$, an atomic site had an x chance to be an S atom and a $(1-x)$ chance to be a Si atom, and hence, the disorder effect for any concentration could be calculated. Here, we defined the probability value of x as the disorder of impurities. As mentioned above, when $x = 1$, it was a periodic doping model; while $x < 1$, the doped model was disordered, and a smaller x indicated a much disordered model.

In our calculations, dopants atoms were placed at appropriate substitutional configurations ($S_1\text{:Si}_{63}$ and $S_1\text{:Si}_{215}$) with the different disorders ($x = 0.1-1$), and the radii (R_a) of the atomic spheres were takes the same value of 1.83 a_B . Besides, other parameters such as band gap E_g of silicon, the width of the impurity band (W_{EI}), distance between the top of the valence band and the bottom of the impurity band (D_{VBM-EI}) and bottom of the conduction band and the top of the impurity band (D_{CBM-EI}) were listed in Table 1.

Table 1. The parameters used in the two ASA model.

	R_a (a_B)	E_g (eV)	W_{EI} (eV)	D_{VBM-EI} (eV)	D_{CBM-EI} (eV)
$S_1\text{:Si}_{63}$	1.83	1.1973	0.6123	0.6449	-0.0599
$S_1\text{:Si}_{215}$	1.83	1.1646	0.2150	0.8544	0.0952

3. Results and discussion

We fabricate 3 kinds of hSi samples in the atmosphere of SF_6 , NF_3 , or N_2 under different laser fluences, and compare the highest optical absorptance from different hSi samples, the results are shown in Fig. 1(a). All the as-irradiated hSi samples exhibit strong broadband optical absorptance compared to the planar crystalline Si. In particular, the SF_6 -hSi has the highest absorptance of $>80\%$ in the whole measurable wavelength range of 0.3–16.7 μm . In comparison, both NF_3 - and N_2 -hSi samples exhibit similar absorptance spectra. In the range of 9–16.7 μm , the absorptance of both samples is $\sim 70\%$, only slightly lower than that of the SF_6 -hSi. However, in the range of shorter wavelength ($<9\ \mu\text{m}$), the optical absorptance of the NF_3 - and N_2 -hSi samples is much

lower than that of the SF₆-hSi, both of which increase gradually from ~30% at 3 μm to ~70% at 9 μm.

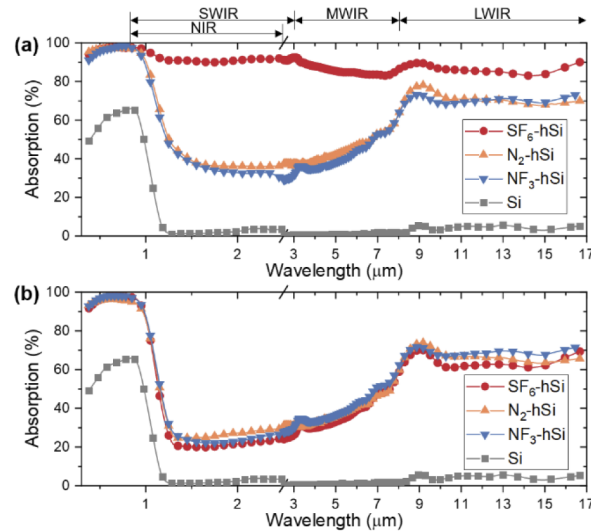


Fig. 1. Optical absorbance spectra of SF₆-, NF₃- and N₂-hSi samples (a) before (as-irradiated) and (b) after annealing.

It is generally acknowledged that the intrinsic absorption contributes to the absorption at <1.1 μm, and meanwhile, the multi-reflectance from the surface structures further highlights the absorption. Furthermore, the impurity level-to-band absorption and free carrier absorption are probably the major mechanisms for the longer wavelength IR than 1.1 μm [32]. Of course, many other factors also influence the IR absorption by different ways. Although both the S and N dopants in the surface layer of the hSi could form various IBs in the Si bandgap, which give rise to the impurity level-to-band absorption [8,33], the doping sites or atomic structures of these impurities in the Si lattices are largely different, which could influence the intensity of the impurity level-to-band absorption. Unlike the S doping that could induce IBs in various structures, only the single-N defects, rather than the N-molecule defects, induce IBs among many atomic structures of N doping in silicon lattices [10,11]. This is probably the reason why the N hyperdoped Si has lower absorbance than the S hyperdoped Si, which also can be observed in previous studies [34]. Therefore, we assign different dopant atoms (S and N) to the large difference of absorption in the spectral range of 1.1–9 μm between SF₆-hSi and NF₃-/N₂-hSi.

The absorbance spectra are remeasured after all samples treated with RTA processing. Figure 1(b) shows that the absorbance of the SF₆-hSi declines sharply to almost the same as that of NF₃-hSi and N₂-hSi in the whole wavelength range, but the absorbance of NF₃-hSi and N₂-hSi is essentially unchanged after the annealing process. For the as-irradiated SF₆-hSi, the presence of strong impurity level-to-band absorption is induced by the interstitial and quasi-substitutional configurations of S doping, which mostly transform into the lowest energy interstitial configurations after annealing and cannot induce any IBs in the bandgap of Si [11]. On the other hand, the sub-bandgap absorbance of NF₃-hSi and N₂-hSi is induced by the single-N defects as the substitutional configurations, which has good thermal stability during the annealing process [10]. Nonetheless, the upper bound of the wavelength for the absorbance induced by the IBs is about 6 μm (0.2 eV) [24]. This means that for the 3 kinds of hSi samples, the remaining absorbance in 6–16.7 μm should attributed to different mechanisms from the impurity level-to-band absorption. Additionally, the extremely non-equilibrium doping process is known

to cause dopants segregation and form larger amount of nanoclusters [22,35]. High temperature thermal annealing reactivation of the doping sulfur from these nanoclusters and further influence the impurity level-to-band absorption [36]. The largely difference of the absorption drops after thermal annealing implies the nanoclusters should not responsible for the longer wavelength absorption. Therefore, according to the previous assumption, the free carrier absorption should be the other main mechanism for the remaining IR absorption after the thermal annealing process [32]. Besides, both the specific surface microstructures and nanoparticles on the micro-spikes' surface are also potential influence factors on the remaining IR absorption after thermal annealing [24,26].

In order to investigate the effects of surface morphology on the optical absorbance, all the hSi samples are observed by the SEM, as shown in Fig. 2. For all the 3 hSi samples, the average height (h) of the quasi-periodic conical spikes on the surface is about 12–14 μm and the spike separation (w) is about 4–4.5 μm , even though the shapes and surface features of the micro-spikes vary for each sample. It should be noted that S and N atoms are doped at a concentration of more than 10^{19} – 10^{20} atoms/ cm^3 in the depth of 200–600 nm beneath the surface, which drops sharply at a deeper depth [5,8,28].

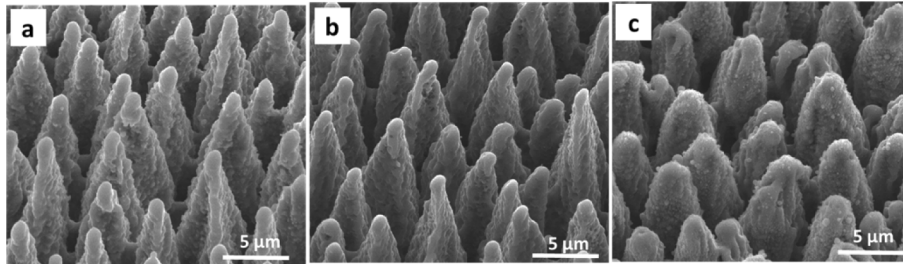


Fig. 2. SEM images of the hSi samples fabricated by fs-laser in (a) SF_6 (b) NF_3 (c) N_2 . All the images were taken at an angle of 45° to the surface.

The quasi-periodic spikes on the specific surface increase the absorption of incident light by reducing reflection and/or increasing the optical path length in a wide wavelength range. The anti-reflection or light trapping effect of the hSi surface is determined by the high (h) and separation (w) of these quasi-periodic spikes, while it is also a function of the wavelength of incident light [24,37]. Only when the wavelength of incident light is shorter than 2 times of spikes' separation ($\lambda < 2w$), multi-reflection among the surface spikes could occur to reduce the total amount of reflected light, which is further reduced by non-normal angle incidence on microstructures [24,37]. Furthermore, a surface layer with graded density appears when the wavelength of incident light is between 2 times of spikes' separation and 2.5 times the spikes' height ($2w < \lambda < 2.5h$). However, the spikes do not affect light trapping when the wavelength of incident light is longer than the height of spikes at 2.5 times ($\lambda > 2.5h$). Therefore, all the hSi samples here are covered by micro-spikes with 4–4.5 μm separation, the multi-reflection should mainly occur in the wavelength $< 9 \mu\text{m}$, and it also causes the gradual variation of the absorption in M–LWIR ($< 28 \mu\text{m}$).

To further investigate the influence of the size of microstructures on the light absorption, the absorbance spectra, for the SF_6 -, NF_3 - and N_2 -hSi samples fabricated with different laser fluences, are presented in Fig. 3. As shown in Fig. 3(a), the optical absorbance of the SF_6 -hSi increases as the height of the surface spikes in a wide wavelength range, which is consistent with the previous report [8]. Figure 3(b) also shows that the average M–LWIR absorption of all the 3 kinds of hSi samples are increasing with the high of spikes in the surface. However, the height of the spikes and doping concentration are closely combined, both of which are increased as the increased laser fluence. Furthermore, although the NF_3 -hSi possesses almost the same

surface morphology compared to the SF₆-hSi, as seen in Fig. 2(a) and (b), it exhibits a 10% lower average M-LWIR absorptance. Although both the NF₃-hSi and N₂-hSi are doped with the same dopant element, they also show different M-LWIR absorptance. Therefore, we can infer that both the surface morphology and the dopants (doping concentration and/or types) influence the M-LWIR absorptance of the hSi.

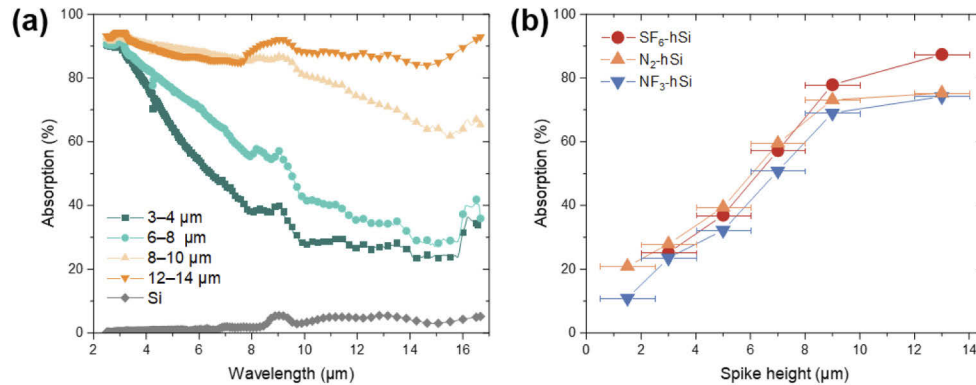


Fig. 3. (a) Absorptance spectra of the SF₆-hSi increase as the height of the spikes in surface; and (b) average M-LWIR absorptance (9–16.7 μm) of the SF₆- NF₃- and N₂-hSi with different heights of spikes. Error bar denotes the uncertainty in determining the spike height.

To further confirm the effects of dopants on the M-LWIR absorption, we perform a chemical etching treatment of SF₆-hSi surface in 10% KOH solution. Both the surface morphology and the doping concentration on the surface are regulated by controlling the etching duration. As seen Fig. 4(a), after etching for 20 s, both the N-SWIR and M-LWIR absorptance declines by about 30%, but the surface morphology (especially the h and w of the spikes) is almost unchanged (left in Fig. 4(b)). This demonstrates that the dopants concentration has a major impact on optical absorptance on the whole range. After the RTA treatment of the 20s-etched sample, the absorptance drops in the wavelength range of <9 μm, but it is almost unchanged in the range of >9 μm. As previously mentioned, the IBs gradually disappear due to annealing which reduces the N-SWIR, whereas the stable M-LWIR absorptance should be attributed to different mechanisms from the impurity level-to-band absorption. As the etching duration increase to 60 s, the surface morphology is completely changed and the spikes almost disappear (right in Fig. 4(b)). The disappearing of S_{2p} peak in the XPS spectrum in Fig. 4(c) implies the S dopants are completely removed away after 40 s etching. And both the N-SWIR and M-LWIR absorptance (Fig. 4(d)) does not further decrease with increasing etching duration. Furthermore, the M-LWIR absorptance remains nearly unchanged from etching of 40 s to 60 s, indicating the M-LWIR is less sensitive to surface morphology.

Although both the surface morphology and the supersaturated dopants have a huge impact on the IR absorptance of hSi, our results confirm that the main mechanism accounting for the M-LWIR absorptance is different from N-SWIR absorption. For the N-SWIR, the impurity level-to-band absorptance induced by the supersaturated dopants is the major mechanism, whereas free carrier absorption should be the main reason for the M-LWIR absorptance. In addition, after 60 s etching, a high absorptance is measured from the hSi compared with the crystalline Si (c-Si) (Fig. 4(a)). Although the dopants should be completely removed, the surface is still covered by microstructures. Thus, the remaining absorptance could be considered as free carrier absorption from the Si substrate enhanced by the surface structure, as the absorptance peaks almost match the predicted vibration modes of c-Si [38].

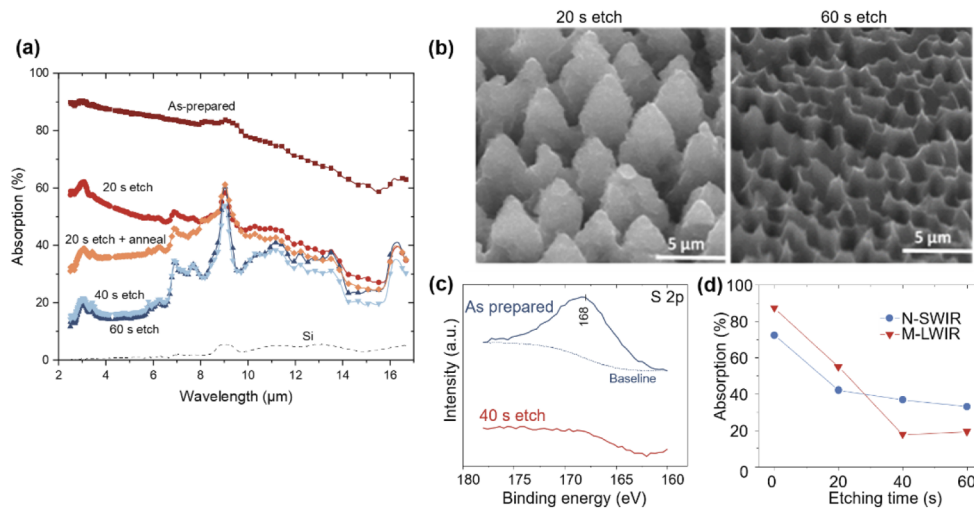


Fig. 4. (a) Absorbance spectra of the SF₆-hSi samples with different post processing steps. (b) SEM images of the SF₆-hSi etched for 20 s and 60 s. (c) XPS spectrum of the as-prepared and 40 s etched samples. (d) Average N-SWIR and M-LWIR absorption as a function of the etching time.

Based on an ideal doping model, which assumes that the impurities are evenly distributed in the silicon lattices, many theoretical calculations of the energy levels for the hSi [11,39]. However, in reality, during the extremely non-equilibrium process induced by fs-laser irradiation, the doped impurities in the hSi surface layer are highly disordered which could not be described by a constant supercell under periodic boundary conditions. Theoretical models structured by the CPA method and implemented in the NANODSIM package give the variational process of the IB in the E_g of silicon with the degree of disorder of impurities. The calculated CPA band structures of the substitutional configurations ($S_1:Si_{63}$ and $S_1:Si_{215}$) with the different disorders ($x = 0.1-1$) in the energy range of -1.3 eV \sim 0.8 eV are shown in Fig. 5. For the higher doping concentration (1.56%) case, shown as in Fig. 5(a), an isolated IB appears in the bandgap of Si due to the supersaturated impurity when $x = 1$, which follows previous calculations without disordered structure. However, the IB shifts closer to the conduction band (CB) as the degree of disorder increases and then hybridized with the CB (when $x \leq 0.7$), indicating that the charge carriers in the IB exhibit CB-like characteristics. Additionally, the IB widens as the disorder increases, and the strongest widening effect occurred when the $x = 0.1$, which is the most closely to the highly disordered of the fs-laser hSi. In Fig. 5(b), when the impurities concentration decrease (for the 0.46% case), although the IB was isolated when the $x \geq 0.5$, it also widens and hybridizes with the CB as the disorder increases ($x \leq 0.4$). The IB widening in the CPA band structures is one of the most important effects that is influenced by the disordered S dopants and induces the hybridization of the IB and CB.

The hybridization of the IB and CB in both of the two doping concentration cases indicated free carriers are generated. And the higher the doping concentration, the easier the hybridization, which also confirms that the introduction of supersaturated dopants significantly increases the concentration of the free carriers. Therefore, upon photon irradiation, the free carrier absorption occurs through the transition of electron energy to a higher energy state within the conduction band [32]. The free carrier absorption depends on the concentration of free carriers, which is affected by the impurity concentration and light wavelength [24]. Thus, the free carrier absorption

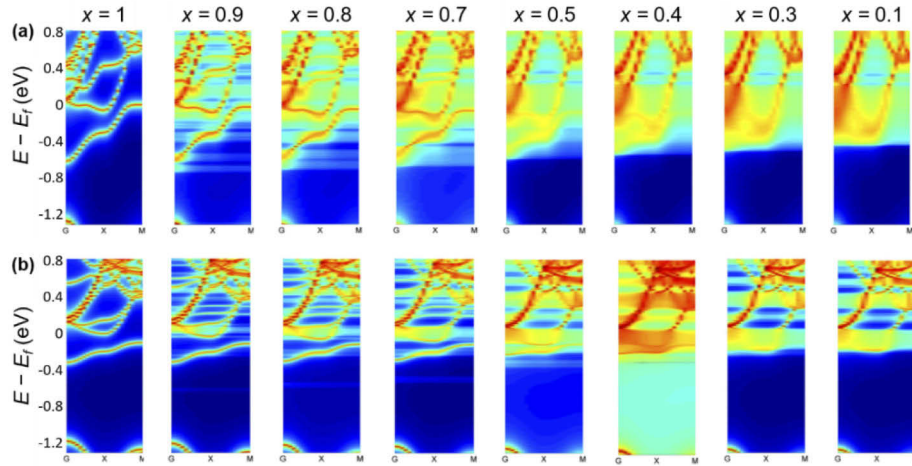


Fig. 5. Band structures of the sulfur atoms' substitutional configurations of (a) $S_1:Si_{63}$ and (b) $S_1:Si_{215}$ with different disorder. The fractional coordinates of the k-points in the Brillouin zone are G (0, 0, 0), X (0.5, 0, 0), M (0.5, 0.5, 0).

induced by the dopants plays an important role in the M–LWIR absorption of the hSi materials. Further investigation on the mechanism of the M–LWIR absorption for the hSi materials, based on the experiment and theoretical results, will provide a specific direction for the research on the longer wavelength absorption of the silicon materials.

4. Conclusion

In conclusion, we systematically study the optical absorption of the SF_6 -, N_2 - and NF_3 -hSi in the wavelength of 0.3–16.7 μm . We confirm that both the surface morphology and the supersaturated dopants influence the IR absorptance of the hSi, and the mechanism for M–LWIR (9–16.7 μm) absorptance is different from the shorter wavelength range. As previously reported, besides the surface morphology, the IBs induced by the supersaturated dopants plays important role in the N–SWIR optical absorption. However, we further confirm that the free carriers absorption should also be a major factor for the IR absorption, especially for the M–LWIR absorption. Taking the SF_6 -hSi for example, theoretical calculations with the CPA method, based on the disordered doping model, demonstrate that the disorder of S atoms in the Si lattices leads to hybridization of the IB with the CB, and increases the concentration of free carriers. The investigation on the M–LWIR absorptance draws a clearer picture for understanding the absorption mechanism of the fs-laser hSi and paves the way for its applications on IR photoelectric devices in telecommunication and security fields.

Funding. National Key Research and Development Program of China (No. 2012CB934200); National Natural Science Foundation of China (No. 51071048); Chinese Academy of Sciences Innovation Fund Project (CXJJ-19S030); Academy of Finland (No. 336145); Foreign Experts Program of Ministry of Science and Technology in China (G2021026027L).

Acknowledgments. Haibin Sun thanks the China Institute of Metrology for the measurement of optical absorptance for this work. Prof. Jun Zhuang from Fudan University is acknowledged for the useful discussion on modeling the disordered doping structure.

Disclosures. The authors declare no conflicts of interest.

Data availability. Data underlying the results presented in this paper are not publicly available at this time but may be obtained from the authors upon reasonable request.

References

1. C. Wu, C. H. Crouch, L. Zhao, J. E. Carey, R. Younkin, J. A. Levinson, E. Mazur, R. M. Farrell, P. Gothoskar, and A. Karger, "Near-unity below-band-gap absorption by microstructured silicon," *Appl. Phys. Lett.* **78**(13), 1850–1852 (2001).
2. L. Du, Z. Wu, Y. Su, R. Li, F. Tang, S. Li, T. Zhang, and Y. Jiang, "Se doping of silicon with Si/Se bilayer films prepared by femtosecond-laser irradiation," *Mat. Sci. Semico. Proc.* **54**(1), 51–56 (2016).
3. M. Tabbal, T. Kim, J. M. Warrender, and M. J. Aziz, "Formation of single crystal sulfur supersaturated silicon based junctions by pulsed laser melting," *J. Vac. Sci. Technol. B* **25**(6), 1847–1852 (2007).
4. D. Recht, M. J. Smith, S. Charnvanichborikarn, J. T. Sullivan, M. T. Winkler, J. Mathews, J. M. Warrender, T. Buonassisi, J. S. Williams, S. Gradečak, and M. J. Aziz, "Supersaturating silicon with transition metals by ion implantation and pulsed laser melting," *J. Appl. Phys.* **114**(12), 124903 (2013).
5. H. Sun, C. Liang, G. Feng, Z. Zhu, J. Zhuang, and L. Zhao, "Improving crystallinity of femtosecond-laser hyperdoped silicon via co-doping with nitrogen," *Opt. Mater. Express* **6**(4), 1321–1328 (2016).
6. I. Umezu, J. M. Warrender, S. Charnvanichborikarn, A. Kohno, J. S. Williams, M. Tabbal, D. G. Papazoglou, X.-C. Zhang, and M. J. Aziz, "Emergence of very broad infrared absorption band by hyperdoping of silicon with chalcogens," *J. Appl. Phys.* **113**(21), 213501 (2013).
7. J. P. Maillo, A. J. Akey, C. B. Simmons, D. Hutchinson, J. Mathews, J. T. Sullivan, D. Recht, M. T. Winkler, J. S. Williams, J. M. Warrender, P. D. Persans, M. J. Aziz, and T. Buonassisi, "Room-temperature sub-band gap optoelectronic response of hyperdoped silicon," *Nat. Commun.* **5**(1), 3011 (2014).
8. C. H. Crouch, J. E. Carey, M. Shen, E. Mazur, and F. Y. Génin, "Infrared absorption by sulfur-doped silicon formed by femtosecond laser irradiation," *App. Phys. A* **79**(7), 1635–1641 (2004).
9. X. Qiu, Z. Wang, X. Hou, X. Yu, and D. Yang, "Visible-blind short-wavelength infrared photodetector with high responsivity based on hyperdoped silicon," *Photonics Res.* **7**(3), 351–358 (2019).
10. Z. Zhu, H. Shao, X. Dong, N. Li, B. Y. Ning, X. J. Ning, L. Zhao, and J. Zhuang, "Electronic Band Structure and Sub-band-gap Absorption of Nitrogen Hyperdoped Silicon," *Sci. Rep.* **5**(1), 10513 (2015).
11. H. Shao, Y. Li, J. Zhang, B.-Y. Ning, W. Zhang, X.-J. Ning, L. Zhao, and J. Zhuang, "Physical mechanisms for the unique optical properties of chalcogen-hyperdoped silicon," *Euro. Phys. Lett.* **99**(4), 46005 (2012).
12. K. Sánchez, I. Aguilera, P. Palacios, and P. Wahnón, "Formation of a reliable intermediate band in Si heavily coimplanted with chalcogens (S, Se, Te) and group III elements (B, Al)," *Phys. Rev. B* **82**(16), 165201 (2010).
13. J. Oh, H. C. Yuan, and H. M. Branz, "An 18.2%-efficient black-silicon solar cell achieved through control of carrier recombination in nanostructures," *Nat. Nanotechnol.* **7**(11), 743–748 (2012).
14. P. Ortega, E. Calle, G. von Gastrow, P. Repo, D. Carrió, H. Savin, and R. Alcubilla, "High-efficiency black silicon interdigitated back contacted solar cells on p-type and n-type c-Si substrates," *Progress in Photovoltaics: Research and Applications* **23**(11), 1448–1457 (2015).
15. J. E. Carey, C. H. Crouch, M. Shen, and E. Mazur, "Visible and near-infrared responsivity of femtosecond-laser microstructured silicon photodiodes," *Opt. Lett.* **30**(14), 1773–1775 (2005).
16. L. Du, Z. Wu, R. Li, F. Tang, and Y. Jiang, "Near-infrared photoresponse of femtosecond-laser processed Se-doped silicon n⁺-n photodiode," *Opt. Lett.* **41**(21), 5031–5034 (2016).
17. X. Liu, S. Ma, S. Zhu, Y. Zhao, X. Ning, L. Zhao, and J. Zhuang, "Light stimulated and regulated gas sensing ability for ammonia using sulfur-hyperdoped silicon," *Sensor. Actuat. B-Chem.* **291**, 345–353 (2019).
18. X. Liu, Y. Zhao, S. Ma, S. Zhu, X. Ning, L. Zhao, and J. Zhuang, "Rapid and Wide-Range Detection of NO_x Gas by N-Hyperdoped Silicon with the Assistance of a Photovoltaic Self-Powered Sensing Mode," *ACS. Sens.* **4**(11), 3056–3065 (2019).
19. X. Liu, Y. Zhao, W. Wang, S. Ma, X. Ning, L. Zhao, and J. Zhuang, "Photovoltaic Self-Powered Gas Sensing: A Review," *IEEE Sens. J.* **21**(5), 5628–5644 (2021).
20. Y. Zhao, X. L. Liu, S. X. Ma, W. J. Wang, X. J. Ning, L. Zhao, and J. Zhuang, "Light-optimized photovoltaic self-powered NO₂ gas sensing based on black silicon," *Sensor. Actuat. B-Chem.* **340**, 129985 (2021).
21. G. J. Feng, Y. Li, Y. Wang, P. Li, J. T. Zhu, and L. Zhao, "Ultrahigh infrared normal spectral emissivity of microstructured silicon coating Au film," *Opt. Lett.* **37**(3), 299–301 (2012).
22. S. Kudryashov, K. Boldyrev, A. Nastulyavichus, D. Prikhod'ko, S. Tarelkin, D. Kirilenko, P. Brunkov, A. Shakhmin, K. Khamidullin, G. Krasin, and M. Kovalev, "Near-far IR photoconductivity damping in hyperdoped Si at low temperatures," *Opt. Mater. Express* **11**(11), 3792–3800 (2021).
23. R. N. T. Dieter, K. Schroder, and John C. Swartz, "Free carrier absorption in silicon," *IEEE J. Solid. St. Circ.* **13**(1), 180–187 (1978).
24. M. J. Sher, Y. T. Lin, M. T. Winkler, E. Mazur, C. Pruner, and A. Asenbaum, "Mid-infrared absorptance of silicon hyperdoped with chalcogen via fs-laser irradiation," *J. App. Phys.* **113**(6), 063520 (2013).
25. X. Dong, N. Li, C. Liang, H. Sun, G. Feng, Z. Zhu, H. Shao, X. Rong, L. Zhao, and J. Zhuang, "Strong Mid-Infrared Absorption and High Crystallinity of Microstructured Silicon Formed by Femtosecond Laser Irradiation in NF₃ Atmosphere," *App. Phys. Express* **6**(8), 081301 (2013).
26. Y. Wang, S. Liu, Y. Wang, G. Feng, J. Zhu, and L. Zhao, "Infrared light absorption of silver film coated on the surface of femtosecond laser microstructured silicon in SF₆," *Mater. Lett.* **63**(30), 2718–2720 (2009).
27. S. Zhang, Y. Li, G. Feng, B. Zhu, S. Xiao, L. Zhou, and L. Zhao, "Strong infrared absorber: surface microstructured Au film replicated from black," *Opt. Express* **19**(21), 20462–20467 (2011).

28. X. Dong, N. Li, Z. Zhu, H. Shao, X. Rong, C. Liang, H. Sun, G. Feng, L. Zhao, and J. Zhuang, "A nitrogen-hyperdoped silicon material formed by femtosecond laser irradiation," *App. Phys. Lett.* **104**(9), 091907 (2014).
29. Q. Lü, J. Wang, C. Liang, L. Zhao, and Z. Jiang, "Strong infrared photoluminescence from black silicon made with femtosecond laser irradiation," *Opt. Lett.* **38**(8), 1274–1276 (2013).
30. Z. Zhu, J. Xiao, H. Sun, Y. Hu, R. Cao, Y. Wang, L. Zhao, and J. Zhuang, "Composition-dependent band gaps and indirect–direct band gap transitions of group-IV semiconductor alloys," *Phys. Chem. Chem. Phys.* **17**(33), 21605–21610 (2015).
31. Y. Ke, K. Xia, and H. Guo, "Disorder scattering in magnetic tunnel junctions: theory of nonequilibrium vertex correction," *Phys. Rev. Lett.* **100**(16), 166805 (2008).
32. C. H. Li, J. H. Zhao, X. Y. Yu, Q. D. Chen, J. Feng, and H. B. Sun, "Fabrication of black silicon with thermostable infrared absorption by femtosecond laser," *IEEE Photon. J.* **8**(6), 6805809 (2016).
33. S. Huang, Q. Wu, Z. Jia, X. Jin, X. Fu, H. Huang, X. Zhang, J. Yao, and J. Xu, "Black Silicon Photodetector with Excellent Comprehensive Properties by Rapid Thermal Annealing and Hydrogenated Surface Assignment," *Adv. Opt. Mater.* **8**(7), 1901808 (2020).
34. S. X. Ma, X. L. Liu, H. B. Sun, Y. Zhao, Y. Hu, X. J. Ning, L. Zhao, and J. Zhuang, "Enhanced responsivity of co-hyperdoped silicon photodetectors fabricated by femtosecond laser irradiation in a mixed SF₆/NF₃ atmosphere," *J. Opt. Soc. Am. B* **37**(3), 730–735 (2020).
35. G. Haberfehlner, M. J. Smith, J. C. Idrobo, G. Auvert, M. J. Sher, M. T. Winkler, E. Mazur, N. Gambacorti, S. Gradecak, and P. Bleuet, "Selenium segregation in femtosecond-laser hyperdoped silicon revealed by electron tomography," *Microsc. Microanal.* **19**(3), 716–725 (2013).
36. B. K. Newman, M. J. Sher, E. Mazur, and T. Buonassisi, "Reactivation of sub-bandgap absorption in chalcogen-hyperdoped silicon," *Appl. Phys. Lett.* **98**(25), 251905 (2011).
37. Y. F. Huang, S. Chattopadhyay, Y. J. Jen, C. Y. Peng, T. A. Liu, Y. K. Hsu, C. L. Pan, H. C. Lo, C. H. Hsu, Y. H. Chang, C. S. Lee, K. H. Chen, and L. C. Chen, "Improved broadband and quasi-omnidirectional anti-reflection properties with biomimetic silicon nanostructures," *Nat. Nanotechnol.* **2**(12), 770–774 (2007).
38. M. Steglich, D. Lehr, S. Ratzsch, T. Käsebier, F. Schrepel, E. B. Kley, and A. Tünnermann, "An ultra-black silicon absorber," *Laser Photonics Rev.* **8**(2), L13–L17 (2014).
39. M. T. W. Elif Ertekin, Daniel Recht, Aurore J. Said, T. B. Michael J, Jeffrey C. Aziz, and Grossman, "Insulator to metal transition in selenium hyperdoped silicon observation and origin," *Phys. Rev. Lett.* **108**(2), 026401 (2012).